Retrieving the phase of diffraction orders generated with tailored gratings

ESTHER NABADDA[1], MARÍA DEL MAR SÁNCHEZ-LÓPEZ[1,2], PASCUALA GARCÍA-MARTÍNEZ[3] AND IGNACIO MORENO[1,4,*]

[1]*Instituto de Bioingeniería, Universidad Miguel Hernández de Elche, 03202 Elche, Spain*
[2]*Departamento de Física Aplicada, Universidad Miguel Hernández de Elche, 03202 Elche, Spain*
[3]*Departamento de Óptica y Optometría y Ciencias de la Visión. Facultat de Física. Universitat de València, 46100 Burjassot, Spain*
[4]*Departamento de Ciencia de Materiales, Óptica y Tecnología Electrónica, Universidad Miguel Hernández de Elche, 03202 Elche, Spain*
**Corresponding author: i.moreno@umh.es*

Received XX Month XXXX; revised XX Month, XXXX; accepted XX Month XXXX; posted XX Month XXXX (Doc. ID XXXXX); published XX Month XXXX

A technique is performed to quantitatively evaluate the intensity and phase of the diffraction orders generated by tailored phase gratings displayed onto a liquid-crystal spatial light modulator (LC-SLM). The SLM displays the grating together with a lens to obtain the Fourier transform. The setup is converted into a polarization common-path interferometer by simply rotating a polarizer. This configuration allows applying a phase-shifting interferometry algorithm to retrieve the phase of the diffraction orders. The quadratic phase arising in the system, which must be subtracted, is calibrated using triplicator gratings of varying periods. Various tailored designs with controlled phase shift between diffraction orders are experimentally tested to prove the advantage and simplicity of the technique. © 2022 Optica

OCIS codes: *(050.0050) Diffraction and gratings; (050.5080) Phase shift; (070.6120) Spatial light modulators; (090.1995) Digital holography.*

http://dx.doi.org/10.1364/OL.99.099999

Diffraction gratings are classical optical elements traditionally used in spectroscopy. The development of optical lithography in the 70's changed their fabrication, offering highly precise control over very large scales, leading to other applications like laser tuning [1] and interferometers [2]. Binary-phase and multilevel gratings were developed in the 90's for laser beam splitting [3]. Later, gratings with continuous phase profiles were designed to produce orders with arbitrary intensity and phase [4]. However, the physical realization of such continuous phase profiles was complicated. They were later demonstrated using the continuous phase modulation provided by a liquid-crystal (LC) spatial light modulator (SLM) [5].

Although these design techniques allow a full control of the complex values at the diffraction orders, most of the research was devoted to control their intensities, and the interest in the phase content was limited to some applications in interferometry [6]. However, polarization diffraction gratings (PDG), gratings that produce diffraction orders with different polarizations, have nowadays become popular. They use continuous phase designs for two orthogonal polarizations, and they can be implemented with LC-SLMs [7], with geometric phase elements [8] or with metamaterials [9]. In all cases, the relative phase between diffraction orders is the key parameter to control the polarization. Therefore, a method for quantitatively measuring the complex-amplitude values of the diffraction orders is of great interest when evaluating the designs of such tailored gratings.

For this purpose, we apply a common-path self-interferometric arrangement of the LC-SLM recently demonstrated with structured light [10]. The system changes from a standard intensity configuration to an interferometer configuration simply by rotating a polarizer. The interferometer configuration implies an additional quadratic phase in the Fourier plane that must be compensated, especially if the observed field is large. Therefore, we here improve the previous system by implementing a calibration procedure based on the optimal triplicator grating design [11].

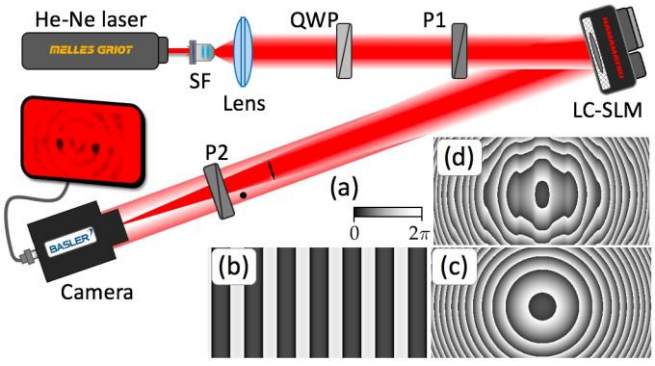

Fig. 1. (a) Scheme of the optical system. SF: spatial filter; QWP: quarter-wave plate; P: linear polarizer. Phase functions displayed on the LC-SLM: (b) Diffraction grating (c) Lens (d) Combined hologram.

Figure 1 shows the experimental setup. A linearly polarized He-Ne laser (Melles-Griot 05-LHP-991, with wavelength $\lambda = 633\ nm$) is spatially filtered and collimated. A quarter-wave plate (QWP) converts it into circularly polarized, so a first linear polarizer (P1) can be rotated without changing the input intensity. The beam illuminates a reflective parallel-aligned LC-SLM (Hamamatsu X10468-01, with 800×600 square pixels, $20\ \mu m$ pixel pitch and 98% fill factor). The reflected beam is directed to a camera detector (Basler scA1390-17fc, with 1390×1038 square pixels of $4.65\ \mu m$ size). A second polarizer (P2) oriented at 45º with respect to the LC director axis is placed in this reflection path.

The SLM displays a phase-only computer-generated hologram (CGH) $\phi_{CGH}(\mathbf{r}) = \phi_G + \phi_L$, $\mathbf{r} = (x, y)$, that combines a grating $g(\mathbf{r}) = \exp[i\phi_G(\mathbf{r})]$ and a converging lens $\phi_L(\mathbf{r}) = \pi r^2 / \lambda f$, where r is the radial coordinate and f is the encoded focal length. The input polarization component parallel to the LC-SLM director axis focuses at the plane located a distance f from the SLM and the field takes the form $G(\mathbf{u}) = \Im[g(\mathbf{r})]$, where $\Im[\cdot]$ denotes the Fourier transform (FT), and $\mathbf{u} = (u, v)$ are the horizontal/vertical spatial frequencies. The spatial coordinates $\mathbf{r}' = (x', y')$ at the Fourier plane are related as $\mathbf{u} = \mathbf{r}' / \lambda f$. Figures 1(b), 1(c) and 1(d) show an example of a grating, the lens and the CGH, where the phases are visualized as the gray levels addressed to the LC-SLM.

In the standard configuration, P1 is aligned parallel to the LC director axis and, consequently, the input beam is fully focused. However, by rotating P1, the system is transformed into a polarization common path interferometer [10]. The polarization component perpendicular to the SLM director axis is unaffected and remains collimated. The second polarizer (P2) makes the two components interfere. The collimated beam acts as the reference, while the focused beam is the test beam. A constant phase can be added to the displayed CGH in order to change the interference condition, thus allowing the application of PSI algorithms to retrieve the phase at the FT plane. Let us note that the employed SLM is free of flicker. Nevertheless, if this were not the case, the related phase fluctuation would yield an additional DC component in the displayed hologram. Since it would not be focused, it would simply add to the background, slightly reducing the interference contrast.

However, since the grating and the lens are both located in the same plane, the optical FT is not exact [12,13] and there is an additional quadratic phase $\phi_Q(r') = -\pi r'^2 / \lambda f$, r' being the radial coordinate at the FT plane. This phase cannot be ignored, especially for measurements far away from the center. In our previous work [10], this phase was simply compensated on the basis of the f value encoded on the CGH. Here, this is quantitatively verified using the optimum phase triplicator grating [11], an analytical design defined by the continuous phase profile:

$$\phi_G(x) = \arctan[a\cos(2\pi x / p)], \qquad (1)$$

where $a = 2.65718\ldots$ and p is the grating period. This grating generates three equally intense zero and ±1 diffraction orders, with a total efficiency that exceeds $\eta = 93\%$. In [14] it was demonstrated that the ±1 orders have a phase shift $\phi_{\pm 1} = \pi / 2$ relative to the zero order. Therefore, the triplicator transmission can be written as

$$g(x) = \exp[i\phi_G(x)] \cong c_0(1 + ie^{+i2\pi x/p} + ie^{-i2\pi x/p}), \qquad (2)$$

with $c_0 \cong \sqrt{0.31}$. Its Fourier transform takes the form

$$G(u) = \Im[g(x)] = c_0[\delta(u) + i\delta(u - u_0) + i\delta(u + u_0)], \qquad (3)$$

with $u_0 = 1/p$. Figure 2 shows experimental results when the SLM displays CGHs with an encoded triplicator of periods $p = n\Delta$, where $\Delta = 20\ \mu m$ (the SLM pixel pitch). We use images of 1024×1024 pixels to calculate the holograms and crop the central 800×600 area to display them on the SLM. Here $n = 1024 / T$ is the period expressed in pixels (px) and we use parameter T to describe the spatial frequency of the gratings. Figure 2 shows results for $T = 8$ and $T = 24$, corresponding to periods of $n = 128\ px$ and $n \simeq 42.7\ px$ respectively. Such large periods ensure that the gratings are not affected by phase quantization. Also, a large focal length $f = 1500\ mm$ is selected to avoid aliasing in the lens function.

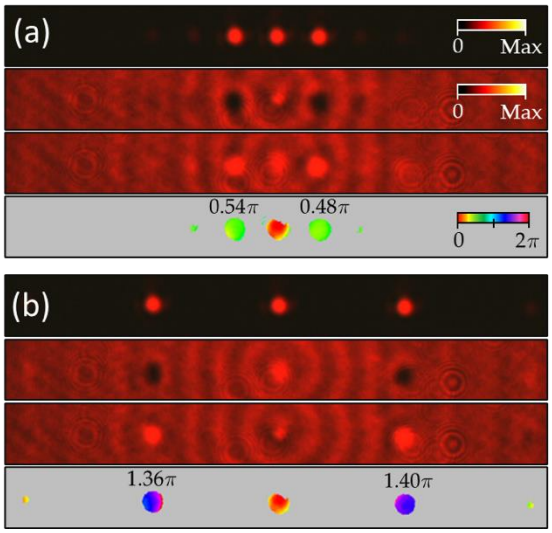

Fig. 2. Intensity (first row), two interferograms with a relative π phase shift (second and third rows) and measured phase (fourth row) for triplicator gratings with different frequency: (a) $T = 8$, (b) $T = 24$.

Each case in Fig. 2 shows four images. The top one is the intensity captured in the standard configuration achieved when P1 is aligned with the SLM director axis. These images verify the generation of three equally intense diffraction orders, with a separation that increases with T. The second and third rows show two interferograms obtained when P1 is rotated. Now the camera shows a background due to the unfocused beam, and the interference is observed at the location of the diffraction orders. Before applying the PSI algorithm, two adjustments are necessary: 1) a constant phase is added to the CGH to put the reference beam in phase with the diffracted field, and 2) P1 is rotated to match the amplitudes of the reference and the diffracted beam, to get a high contrast. The two interferograms shown in each case in Fig. 2 are obtained by adjusting the constant phase to provide destructive and constructive interference in the ±1 orders respectively, as viewed in the corresponding dark and bright spots.

By applying additional constant phase steps, the phase difference between orders can be retrieved using classical PSI algorithms [10]. The result is displayed on the fourth row in each case, where a color code enables to distinguish these phases from the CGHs. The

experimentally measured phases are presented in the range $[0,2\pi)$ and only on the pixels where the intensity is significative, with values over 5% of the maximum. The phase indicated on each order is the average value over the significative pixels, relative to the phase of the zero order, which is taken as the reference. These averaged values show a standard deviation below 0.03π in most of the measured diffraction orders. According to [14], the phase between the zero order and the ±1 orders must be $\pi/2$. However, the interference condition shown in the interferograms in Fig. 2 is observed to change with T, thus denoting an extra phase. Namely, the quadratic phase caused by the non-perfect FT configuration.

The procedure was repeated for different T values, and for triplicators diffracting in vertical direction and the difference with respect the theoretical value $\pi/2$ was calculated. The graph in Fig. 3 shows the result as a function of the radial coordinate, expressed in pixels of the camera, where the phase function was unwrapped. The curve matches the expected quadratic profile with a correlation coefficient of $R^2 = 0.9987$. The inset shows $\phi_Q(\mathbf{r}')$ on the complete area of the camera, reaching around 20π at the corners. Figure 3(b) shows the intensity when a horizontal and a vertical triplicators are combined, thus yielding nine equally intense diffraction orders. However, their phase content is different, as shown in the interferogram in Fig. 3(c). While the ±1 orders along horizontal and vertical directions are $\pi/2$ phase-shifted with respect to the central order, the four diagonal orders are π phase-shifted, a situation that was indirectly verified in [14] with a geometric phase grating regarding the polarization changes. Here, the experimental phase (Fig. 3(d)) retrieved from PSI (after compensating the quadratic phase) provides a direct measurement that agrees very well with the expected result.

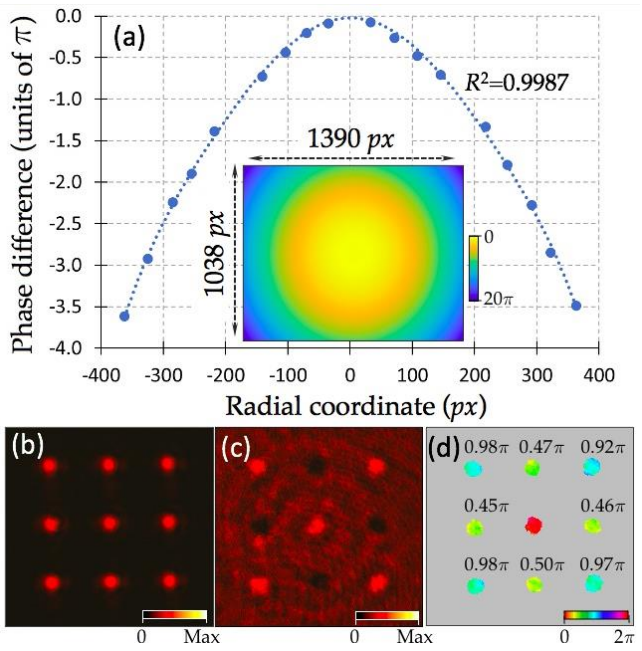

Fig. 3. (a) Experimental quadratic phase profile measured at the FT plane. The inset shows its values at the complete area of the camera array. Nine diffraction orders generated by two crossed triplicators with $T = 12$: (b) intensity, (c) interferogram and (d) phase.

Once the quadratic phase is determined, the procedure can be applied to other gratings. As a first example the detour phase caused by a lateral shifting of the grating is visualized. If the grating $g(x)$ is displaced with respect to the lens by Λp, the FT is transformed to $\Im\{g(x-\Lambda p)\} = G(u)\exp(i2\pi u\Lambda p)$. This additional linear phase changes the phase of the triplicator ±1 orders $(u = \pm 1/p)$, so their phases relative to the zero order become $\phi_{\pm 1} = (\pi/2) \pm 2\pi\Lambda$.

Figure 4 shows the results for gratings with $T = 16$. Figure 4(a) illustrates the CGH functions when the triplicator grating already presented in Fig. 1(d) is displaced by $\Lambda = 1/4$, $\Lambda = 1/2$ and $\Lambda = 3/4$. The intensity distribution (Fig. 4(b)) does not change with Λ. However, the measured phases do change. Figure 4(c) shows the result for the centered grating $(\Lambda = 0)$, where values very close to those expected $\phi_{\pm 1} = \pi/2$ are retrieved. For $\Lambda = 1/4$, phases should change to $\phi_{+1} = \pi$ and $\phi_{-1} = 0$. The experimental values confirm this result, where now the -1 order is in phase with the zero order. On the contrary, for a half-period displacement $(\Lambda = 1/2)$ there is an additional $\pm\pi$ phase-shift at the ±1 orders, thus $\phi_{\pm 1} = 3\pi/2$. Finally, for $\Lambda = 3/4$, the situation is inverted with respect to $\Lambda = 1/4$. In all cases, the measured phases agree well with the expected values.

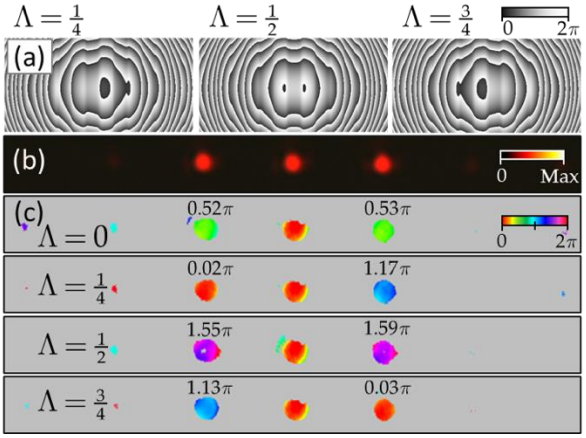

Fig. 4. (a) CGH displayed onto the SLM for triplicator gratings with $T = 16$ and lateral displacements $\Lambda = 0$, $\Lambda = 1/4$, $\Lambda = 1/2$ and $\Lambda = 3/4$. Experimental distributions (b) intensity, and (c) phase.

Finally, two continuous phase gratings are designed to provide a relative intensity and phase shift between orders. The design follows the procedure described in [5] based on the theory of optimum laser beam-splitting gratings [4]. This procedure consists of determining a continuous phase function $\varphi(x)$ that generates a desired pattern of diffraction orders, whose complex amplitude is defined by the Fourier series coefficient:

$$c_k = \sqrt{i_k}\exp(i\beta_k) = \frac{1}{2\pi}\int_{-\pi}^{+\pi}\exp[i\varphi(x)]\exp(-ikx)dx, \qquad (4)$$

k denoting each of the target orders. The design procedure consists in selecting the N desired target orders and defining the desired relative (i_k, β_k) values. Then a function $s(x)$ is defined as

$$s(x) = \sum_{k\in N}\mu_k\exp(i\alpha_k)\exp(i2\pi kx/p), \qquad (5)$$

where (μ_k, α_k) are numerical values of the amplitude and phase of each harmonic component of $s(x)$. These values are determined such that the phase-only function $\exp[i\varphi(x)] = s(x)/|s(x)|$ fulfills the conditions imposed on (i_k, β_k) with the highest possible diffraction efficiency η, defined as the ratio between the sum of intensities at the target diffraction orders relative to the total intensity. More details about can be found in [4,5].

We designed two gratings: Grating 1 is asymmetric with three target orders $k = +2$ and $k = \pm 1$, with intensities $i_{+2} = 2i_{+1} = 2i_{-1}$ and phase shifts $\pi/2$ and π of the second and negative first orders with respect to the first order. Grating 2 has target orders $k = \pm 3$ and $k = \pm 1$, all with the same intensity, and where orders $+3$ and -1 are in phase with the first order, while order -3 has a π phase-shift. Table 1 gives the numerical values of the imposed restrictions relative to the first order, the (μ_k, α_k) parameters and the nominal efficiency. Figure 5(a) shows one period of the continuous phase profiles $\varphi(x)$ for these gratings.

Table 1. Parameters of tailored gratings

GRATING 1			$\eta = 85.3\%$
Target orders	$k = -1$	$k = +1$	$k = +2$
i_k / i_{+1}	1	1	2
$\beta_k - \beta_{+1}$	π	0	$\pi/2$
μ_k	0.9633	0.8189	1.2160
α_k	5.4613	2.3491	3.8993

GRATING 2				$\eta = 86.4\%$
Target orders	$k = -3$	$k = -1$	$k = +1$	$k = +3$
i_k / i_{+1}	1	1	1	1
$\beta_k - \beta_{+1}$	π	0	0	0
μ_k	1.5705	3.4063	5.1173	4.5725
α_k	4.8551	1.7143	1.7136	1.7141

Figure 5 shows the results of Grating 1 and Grating 2. For the first design we also display the complex-conjugated version (Grating 1CC). The intensity and phase of the diffraction orders were measured for gratings with $T = 16$. They show the generation of the target diffraction orders with the desired restrictions. For instance, Grating 1 shows a second order more intense that two equally intense ±1 orders (a weak zero order is also visible). The phase values are presented relative to the first order for Grating 1 and 2 and also bear a very good agreement with the design values. Figure 5(c) shows the result for Grating 1CC which shows the reversed intensity pattern and opposite phases as that in Fig. 5(b). In this case the phase is presented relative to the minus first order.

In summary, we applied a simple experimental technique to experimentally retrieve the phase of diffraction orders generated with tailored diffraction gratings. The technique is based on a self-interferometer configuration of a LC-SLM, where the display is used simultaneously to implement the grating, a lens, and the phase-shift bias required in PSI algorithms. The experimental results confirm the designs and proves the usefulness of the technique to test tailored diffraction gratings before their fabrication with other advanced methods. This can be of particular interest in geometric-phase gratings, where the phase-shift between orders is of great relevance for their polarization-diffraction properties.

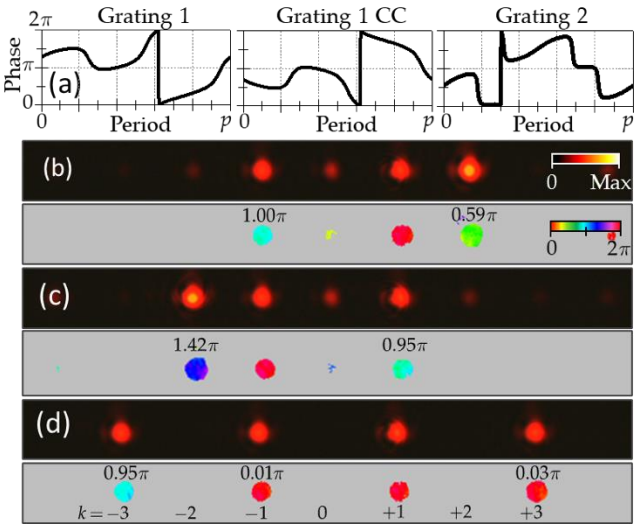

Fig. 5. (a) Phase profiles for three grating designs. (b) Experimental intensity and phase for: (b) Grating 1. (c) Grating 1CC. (d) Grating 2.

Funding. This work received financial support from Ministerio de Ciencia e Innovación, Spain (ref.: PID2021-126509OB-C22) and Generalitat Valenciana (ref. CIAICO/2021/276). EN acknowledges a grant from Generalitat Valenciana (ref. GRISOLIAP/2020/004).

Disclosures. The authors declare no conflicts of interest.

Data availability. Data underlying the results presented in this paper are not publicly available at this time but may be obtained from the authors upon reasonable request.

References

1. N. Bonod and J. Neauport, Adv. Opt. Photon. **8**, 156 (2016).
2. F. Cheng and K. Fan, Appl. Opt. **50**, 4550 (2011).
3. J. N. Mait, J. Opt. Soc. Am. A **7**, 1514 (1990).
4. L. A. Romero and F. M. Dickey, Prog. Optics **54**, 319 (2010).
5. J. Albero, J. A. Davis, D. M. Cottrel, C. E. Granger, K. R. McCormick and I. Moreno, Appl. Opt. **52**, 3637 (2013).
6. C. M. B. Cordeiro, L. Cescato, A. A. Freschi and L. Li, Opt. Lett. **28**, 683 (2003).
7. J. A. Davis, I. Moreno, M. M. Sánchez-López, K. Badham, J. Albero and D. M. Cottrell, Opt. Express **24**, 907 (2016).
8. J. Kim, Y. Li, M. N. Miskiewicz, C. Oh, M. W. Kudenov and M. J. Escuti, Optica **2**, 958 (2015).
9. N. Rubin, A. Zaidi, M. Juhl, R. P. Li, J. P. B. Mueller, R. C. Devlin, K. Leósson and F. Capasso, Opt. Express **26**, 21455 (2018).
10. E. Nabadda, P. García-Martínez, M. M. Sánchez-López and I. Moreno, Front. Phys. **10**, 920111 (2022).
11. F. Gori, M. Santarsiero, S. Vicalvi, R. Borghi, G. Cincotti, E. Di Fabrizio, M. Gentili, Opt. Commun. **157**, 13 (1998).
12. J. W. Goodman, *Introduction to Fourier optics*, 3rd edt. Robert & Company Publishers (2004).
13. I. Moreno, M. M. Sánchez-López, C. Ferreira, J. A. Davis and F. Mateos, Eur. J. Phys. **26**, 261-271 (2005).
14. D. Marco, M. M. Sánchez-López, A. Cofré, A. Vargas and I. Moreno, Opt. Express **27**, 14472 (2019).

References (complete record)

1. N. Bonod and J. Neauport, "Diffraction gratings: from principles to applications in high-intensity lasers", Adv. Opt. Photon. **8**(1), 156-199 (2016).
2. F. Cheng and K. Fan, "Linear diffraction grating interferometer with high alignment tolerance and high accuracy", Appl. Opt. **50**(22), 4550-4556 (2011).
3. J. N. Mait, "Design of binary-phase and multiphase Fourier gratings for array generation", J. Opt. Soc. Am. A **7**(8), 1514-1518 (1990).
4. L. A. Romero and F. M. Dickey, "The mathematical theory of laser beam-splitting gratings", Prog. Optics **54**, 319–386 (2010).
5. J. Albero, J. A. Davis, D. M. Cottrel, C. E. Granger, K. R. McCormick and I. Moreno, "Generalized diffractive optical elements with asymmetric harmonic response and phase control", Appl. Opt. **52**(15), 3637-3644 (2013).
6. C. M. B. Cordeiro, L. Cescato, A. A. Freschi and L. Li, "Measurement of phase differences between the diffracted orders of deep relief gratings", Opt. Lett. **28**(9), 683-685 (2003).
7. J. A. Davis, I. Moreno, M. M. Sánchez-López, K. Badham, J. Albero and D. M. Cottrell, "Diffraction gratings generating orders with selective states of polarization", Opt. Express **24**(2), 907-917 (2016).
8. J. Kim, Y. Li, M. N. Miskiewicz, C. Oh, M. W. Kudenov and M. J. Escuti, "Fabrication of ideal geometric-phase holograms with arbitrary wavefronts", Optica **2**(11), 958-964 (2015).
9. N. Rubin, A. Zaidi, M. Juhl, R. P. Li, J. P. B. Mueller, R. C. Devlin, K. Leósson and F. Capasso, "Polarization state generation and measurement with a single metasurface", Opt. Express **26**(17), 21455-21478 (2018).
10. E. Nabadda, P. García-Martínez, M. M. Sánchez-López and I. Moreno, "Phase-shifting common-path polarization self-interferometry for evaluating the reconstruction of holograms displayed on a phase-only display", Front. Phys. **10**(1), 920111 (2022).
11. F. Gori, M. Santarsiero, S. Vicalvi, R. Borghi, G. Cincotti, E. Di Fabrizio, M. Gentili, "Analytical derivation of the optimum triplicator", Opt. Commun. **157**(1), 13-16 (1998).
12. J. W. Goodman, *Introduction to Fourier optics*, 3rd edt. Robert & Company Publishers (2004).
13. I. Moreno, M. M. Sánchez-López, C. Ferreira, J. A. Davis and F. Mateos, "Teaching Fourier optics through ray matrices," Eur. J. Phys. **26**, 261-271 (2005).
14. D. Marco, M. M. Sánchez-López, A. Cofré, A. Vargas, and I. Moreno, "Optimal triplicator design applied to a geometric phase vortex grating", Opt. Express **27**(10), 14472-14486 (2019).